Manipulability Analysis of a Tree Type Humanoid Upper-Body Robot with Dual Redundant Arms

Dr. Shifa Sulaiman*
Mechatronics/Robotics Laboratory, Mechanical Engineering Department
National Institute of Technology, Calicut, India-673601
Email: shifa_p170114me@nitc.ac.in
Contact No: +91 7561073920

Dr. Sudheer A P
Mechatronics/Robotics Laboratory, Mechanical Engineering Department
National Institute of Technology, Calicut, India-673601
Email: apsudheer@nitc.ac.in
Contact No: +91 9961450987

Dr. Santhakumar Mohan
Robotics Laboratory, Mechanical Engineering Department
Indian Institute of Technology, Palakkad, India- 678623
Email: santhakumar@iitpkd.ac.in
Contact No: +91 4923226434

Dr. Evgeni Magid**
Laboratory of Intelligent Robotics Systems (LIRS)
Institute of Information Technology and Intelligent Systems,
Kazan Federal University, Kazan, Russia- 420008
Email: magid@it.kfu.ru
Contact No: +7 8432065233

Abstract – Manipulability analysis of humanoid robots with redundant arms is difficult due to the presence of large number of degrees-of-freedom (dof). Most researchers address manipulability issues without considering the effects of joint limits, obstacles and singular spaces in a Cartesian workspace. Hence, development of an accurate manipulability analysis technique, which can increase task performance by considering the above-mentioned issues is crucial for completing cooperative and non-cooperative tasks. Our paper proposes a new approach for determining manipulability measurements of a humanoid robot with redundant arms doing coordinated and non-coordinated tasks by analysing manipulability ellipsoids constructed through a desired trajectory. Penalty functions for compensating joint limits and avoiding obstacle regions are multiplied along with a Jacobian matrix to generate an Augmented Jacobian matrix. Manipulability ellipsoids determined using the Augmented Jacobian for individual configurations are compared with desired manipulability ellipsoids for finalizing the joint solutions. The advantages of proposed approach over conventional approach and significance of employing proposed approach for updating joint configurations are presented in this paper. The experimental validation of the proposed method using a developed humanoid robot is also given in this paper.

- **Additional affiliation: Institute of Electronics and Mathematics (MIEM HSE) / School of Electronic Engineering National Research University Higher School of Economics, Moscow, Russia-101000

1. Introduction and Background

Upper-body humanoid robots with redundant dual arms have gained popularity in recent years due to their adaptability to interact with human environment in various fields. Humanoid robots with mobile platforms are broadly used for training purposes [1] - [2], personal assistance [3] - [4], health care [5] - [6], entertainment [7] - [8] and space exploration [9] - [10]. Manipulability analysis helps to monitor various configurations of a humanoid robot and select suitable configurations for completing a given task with less computational effort. However, most of the conventional manipulability analysis approaches are inaccurate for determining dexterity of redundant arms in the presence of obstacles and joint constraints. An accurate manipulability analysis approach can improve the task performance by taking the aforementioned issues into account while performing cooperative and non-cooperative tasks.

Several manipulability analysis techniques were already developed and implemented for serial chain manipulators and humanoid robots. Manipulability analysis of redundant arms using a visual servoing technique was carried out in [11]. Robot singularities, trajectory optimization, and issues related to joint solution convergences were also addressed in this work. Visual features of workspace images and Damped Least Square (DLS) approaches were implemented for reducing robot singularities. Neha and Shrivastava [12] presented manipulability measurements of a robotic hand using a statistical approach and studied a range of angles for maximizing manipulability measurements. The results aided in determining most appropriate finger postures inside the workspace. The proposed method can be used for evaluating redundancy of a serial chain robot. A comprehensive methodology for optimising joint configurations of a manipulator for desired tasks was explained by Patel *et al.* [13]. Manipulability measurements were determined for finalizing joint configurations for grasping objects. An application of manipulability measurements for determining optimal postures of various mechanisms and manipulators (such as SCARA and PUMA) were discussed. Freddi *et al.* [14] presented a method to derive a relative Jacobian for a cooperative dual-arm robot. The authors proposed a manipulability analysis method for a cooperative redundant manipulator by considering the mechanism as a single manipulator using the relative Jacobian approach. The Jacobian null space technique was employed for resolving redundancy. Case studies of two planar redundant manipulators implementing the proposed method were carried out. Chan *et al.* [15] focused on avoiding extreme limits of joint angles while performing a task using redundant arms. A weighted least norm-based method was employed for determining suitable configurations for avoiding joint limits and collision possibilities during tasks.

Manipulability measurements of a dual-arm manipulator and parameters influencing manipulability of two cooperative robots were discussed in [16]. Three different manipulability indices were developed for analyzing the kinematic manipulability of redundant robots. Manipulability analysis of a 7 degrees-of-freedom (dof) arm for tracking eye motions of a patient based on manipulability ellipsoids was given by Zhang *et al.* [17]. The method aided to avoid singularity regions during operations of the manipulator. Chiriatti *et al.* [18] presented a cobotic system for rehabilitation sessions optimised using manipulability measurements. Manipulability ellipsoids for human arm motions and a cobot were plotted and compared using a manipulability index. The position of the cobot with respect to patient position was determined based on the manipulability index. Choi *et al.* [19] determined optimal postures of redundant manipulators for carrying out a task using manipulability ellipsoid based method. The manipulability ellipsoid was plotted and used for optimising the trajectory by comparing it with directions of axes of desired manipulability ellipsoids. The manipulability analysis of a teleoperated robot for surgical applications in [20] introduced a manipulability index to enhance the performance of coordinated motions of master-slave robots, which improved the slave robot controllability and avoided singularities during task. The proposed strategy can be applied to enhance the design and trajectories of a slave robot.

Lachner *et al.* [21] presented a relation between types of coordinates and manipulability measurements of a manipulator. Dynamic manipulability measurements of an arm with 8 dof was obtained using tensor geometry. Manipulability ellipsoids of the robot were determined and used for analysing the dexterity of the robot arm. Translational velocity and rotational velocity ellipsoids used for determining singularity of a robotic arm was demonstrated by Zhang *et al.* [22]. The singular configurations were verified based on the values of condition number and manipulability measurement. Zhu *et al.* [23] illustrated about the design and manipulability analysis of a 6 dof manipulator used for surgical applications. Manipulability measurements and singularity of the arm were analysed based on monte Carlo method. Isma [24] discussed about a trajectory planning strategy based on Manipulability Percentage Index. An optimal trajectory was calculated based on the manipulability measurement and simulation studies were carried out to prove the advantages of the proposed method. Dufour

and Suleiman [25] discussed about a method for maximizing the manipulability index during the solution of inverse kinematics for a redundant manipulator. Jacobian based formula was integrated into manipulability measurement to obtain optimal joint configurations for carrying out a task.

Potential functions were introduced by Vahrenkamp *et al.* [26] to avoid joint limits, obstacles and self-collisions during motion of manipulators. This method was suitable for determining manipulability of redundant arms, avoiding joint limits and obstacles in a Cartesian workspace. The optimum grasp poses of end effectors can be determined based on the proposed method. Bicchi *et al.* [27] developed a numerical tool for determining manipulability of dual arm robots. The mobility and differential kinematics of robotic dual arms were analysed. Manipulability ellipsoids for different robotic systems were compared to determine optimal configurations of arms to carry out a task. The proposed work can be extended to force/ torque and dynamic manipulability ellipsoids evaluation during tasks. Pose confirmation for a humanoid robot based on manipulability ellipsoids was presented by Shen *et al.* [28]. The upper limb redundancy of the humanoid arm was studied by incorporating different loading conditions. An index for stability known as arm posture stability index (APSI) was introduced in this work. Swivel angles of the humanoid arm were used as a reference for determining APSI values of various arm postures. Determination of Grasp poses for manipulating an object with manipulability ellipsoid parameters were studied by Kumar and Mukherjee [29]. The methodology searched for desired manipulability ellipsoid configurations to complete a given task accurately. The search was based on reduction of a geodesic distance between current and goal manipulability matrices. A geometry based method employed for finalizing postures of a master-slave robotic system based on manipulability ellipsoid was given by Rozo *et al.* [30]. The slave robot tried to imitate motions of the master robot by matching manipulability ellipsoids of various postures. An extended manipulability measurement by incorporating different constraints was illustrated by Vahrenkamp and Asfour [31] and considered effects of joint limits, obstacle avoidance and workspace characteristics. Grasp planning and manipulability analysis by incorporating a penalty function using the proposed scheme were validated using ARMAR III robot [32].

Joint limits and obstacle regions related manipulability issues are compensated in this work by introducing a penalty function along with respective Jacobians to generate an Augmented Jacobian matrix. Augmented Jacobian for coordinated and non-coordinated arm motions are determined using relative Jacobian and space Jacobian respectively. Desired manipulability ellipsoids for traversing a trajectory are plotted using eigen values and vectors derived from the Augmented Jacobian matrix. Manipulability ellipsoids are plotted for finding optimal configurations of upper body section of the humanoid robot by avoiding extreme joint values and obstacles from an available set of joint configurations. Directional vectors of major axes of desired manipulability ellipsoids for traversing a given trajectory is taken as a reference to determine similarity between desired and obtained manipulability ellipsoids. Joint configurations of redundant arms are finalized when the desired and current manipulability ellipsoid become similar with respect to the above-mentioned criterion. An experimental validation of the proposed approach is carried out using the previously fabricated humanoid robot [33].

The rest of the paper is organized as follows. Section 2 briefly describes the humanoid robot. A derivation of space and relative Jacobian matrices are explained in Section 3. Manipulability analysis of humanoid robot using a penalty function is given in section 4. Section 5 presents results of experimental validation using wheeled humanoid robot. Finally, we conclude in Section 6.

2. A humanoid robot description

We modelled the upper body humanoid robot with a mobile platform using screw theory formulations [34]. The 15 dof upper body humanoid was designed with 3 dof hip, 2 dof neck and 5 dof arms each (Figure 1) using biomechanics data of a 1.6 m tall human [35], which dimensions are presented in Table I.

2.1 Fabrication of the humanoid robot

The conceptual model was first designed based on bio mechanics data and evaluated for determining the robot workspace. Various singularity and void spaces were identified inside the workspace during the validation of initial conceptual model in softwares. The presence of singular and void spaces decreased the robot dexterity. Hence, the initial conceptual model was redesigned to reduce singular and void spaces. The final conceptual model and fabricated model are shown in figures 2 (a) and (b) respectively.

Structural analysis was carried out for determining stresses and deformations occurring in the humanoid robot model. A combined load of 5 kg was given as an initial load for calculating final dimensions of humanoid links within 1.5 safety factor. The proposed model of the tree type humanoid robot with redundant arms and the mobile platform were fabricated to evaluate the theoretical results. Based on the structural analysis, aluminium was selected for the upper body. All joints of the

upper body were revolute, the upper body links were arranged in a way that ensures kinematic and dynamic stability of the system. The neck carries less load as compared to other parts of the robot and therefore it was fabricated using an acrylic material. The mobile platform was fabricated using cast iron. The mobile platform employed two standard wheels and two caster wheels (which improved the base balance).

3. Derivation of space Jacobian and relative Jacobian matrices

In this section, derivation of a space Jacobian for analysing non-coordinated tasks and derivation of a relative Jacobian for analysing coordinated tasks carried out by redundant arms are described. Consider a 6x1 vector v, which contains a relative pose of the end effector joint as given in equation (1):

$$v = \left[\frac{p_i}{\omega_i}\right], (1)$$

where p_i is a 3x1 position vector and ω_i is a 3x1 relative rotation vector with respect to a definite pose of the end effector joint. Equation (1) can also be rewritten as given in equation (2):

$$v = J\dot{q}, (2)$$

where J is a 6xn space Jacobian matrix [36] for n joints and $\dot{q}$ is the joint velocity vector. In the space Jacobian matrix, each column of the Jacobian was derived with respect to fixed frames that corresponds to each joint screw axis. The Jacobian was non-square and hence was not invertible for redundant robots. The redundant robot Jacobian is presented in equation (3) and the manipulability measurement [36] for non-coordinated tasks is given in equation (4):

$$J_j = J \times J^T, (3)$$

$$J_m = \sqrt{J \times J^T}, (4)$$

A relative Jacobian matrix [37] was considered for obtaining manipulability measurements of redundant arms carrying out cooperative tasks. During a coordinated task, when two arms jointly performed the task (for example, picking and placing an object), two redundant arms of humanoid robot were considered as a single chain with a common end effector for deriving the relative Jacobian along with a wrench transformation matrix [14]. The relative Jacobian matrices were derived with respect to the end effector pose of the left hand for the coordinated motion of the two arms. The joints of the tree type humanoid robot were divided into three branches for the analysis. Branch 1 (B_{r1}) consisted of 3 dof hip joints and 2 dof neck joints. Branch 2 (B_{r2}) and Branch 3 (B_{r3}) consisted of 5 joints corresponding to the right arm and the left arm, respectively from the shoulder joints to the end effector joints. The mobile platform module is represented as (B_{rw}). The relative Jacobian of B_{r1} and B_{r3} branches is given in equation (5):

$$R_{j1} = \left[-\delta_{Br3}\sigma_{Br3}\gamma_{Br3} \quad \sigma_{Br1}\gamma_{Br1}\right], (5)$$

The relative Jacobian of B_{r2} and B_{r3} branches is given in equation (6):

$$R_{j2} = \left[-\delta_{Br3}\sigma_{Br3}\gamma_{Br3} \quad \sigma_{Br2}\gamma_{Br2}\right], (6)$$

The relative Jacobian of the humanoid upper body considering all three branches is formulated as given in equation (7):

$$R_j = \left[-\delta_{Br3}\sigma_{Br3}\gamma_{Br3} \quad 0 \quad \sigma_{Br2}\gamma_{Br2}\right], (7)$$

Where $\delta_{Bri} = \begin{bmatrix} I & -\tilde{A} \\ 0 & I \end{bmatrix}$ is known as the wrench transformation matrix(6x6), I is the 3x3 identity matrix and $\tilde{A}$ is the 3x3 skew-symmetric matrix of position vectors between the end effectors. If $A = \begin{bmatrix} P_x & P_y & P_z \end{bmatrix}^T$, then

$\tilde{A} = \begin{bmatrix} 0 & -p_z & p_y \\ p_z & 0 & -p_x \\ -p_y & p_x & 0 \end{bmatrix}$ is the skew-symmetric matrix. $\sigma_{Bri} = \begin{bmatrix} \dot{R} & 0 \\ 0 & \dot{R} \end{bmatrix}$ is the 6x6 diagonal rotation matrix and $\dot{R}$ represents the rotation transformation matrix, which transforms the Jacobian from the base frame to the end-effector frame of the reference branch. γ_{Bri} is the corresponding Jacobian matrix of each branch. Branch 3 (left arm) was multiplied with the wrench transformation matrix due to a moving reference frame attached to the left arm's end-effector frame. The individual Jacobian

matrices of each branch were derived in a space Jacobian form. Since in this paper, cooperative tasks were carried out by dual arms, parameter of branch B_{r1}(the second element) is not considered in equation (7). The manipulability measurement of the humanoid robot derived using the relative Jacobian method incorporating the wrench transformation matrix is given in equation (8)

$$J_R = \sqrt{R_j R_j^T} , (8)$$

This manipulability measurement was used for analysing manipulability and force ellipsoids to determine a range of motions corresponding to each particular configuration of the redundant arms. A manipulability ellipsoid relates joint velocities to Cartesian velocities. Dexterity of a robotic system is proportional to volume of the manipulability ellipsoid. The length corresponding to each axis of the manipulability ellipsoid represents the range of motion along that particular direction. Let λ_i and μ_i represent eigenvalues and eigenvectors of manipulability measurements. The length of ellipsoid's axis is given by $\sqrt{\lambda_i}$ and the direction of the axis is μ_i. Another type of ellipsoid is a force ellipsoid, which relates joint forces to Cartesian forces for analysing force acting in Cartesian space. The length of axes of the force ellipsoid can be determined from a manipulability ellipsoid. The lengths of axes of the force ellipsoid are given by $1/\sqrt{\lambda_i}$. Principal axes of the force ellipsoid are aligned with principal axes of the manipulability ellipsoid as shown in figure 3. In this paper, force ellipsoids are plotted along with manipulability ellipsoids to represent the direction of force acting on the manipulator.

4. Manipulability analysis of the upper body using Penalty functions

Most works related to manipulability analysis do not consider effects of joint limits, presence of obstacles in a workspace and potential self-collisions. Our approach introduced two penalty functions to compensate for the above-mentioned effects and calculated the manipulability measurements of redundant arm configurations of the upper body humanoid robot in clustered environments. These penalty functions were added along with respective Jacobians to form an Augmented Jacobian. Augmented Jacobian was used for plotting manipulability ellipsoid to determine joint solutions of redundant arms by incorporating the effects of joint constraints and collisions. These manipulability ellipsoids were compared with desired manipulability ellipsoids to finalize the joint solutions for traversing the desired trajectory.

4.1 Joint limit penalty function

The joint limit penalty function considered current distance to joints' limits and penalized the distance by considering each column of the Jacobian, one at a time for cooperative and non-cooperative tasks. We employed an improvised form of penalty function that was introduced in [15] and considered a lower joint limit and an upper joint limit. The motions of joints were constrained to avoid extreme joint values using a positive definite weighting matrix, W_p. The weighted normal form of a joint velocity vector, V_{wp} with joint velocity, V is given by the following equation (9):

$$V_{wp} = \sqrt{V^T W_p V} , (9)$$

where W_p is a $6n$ x $6n$ symmetric and diagonal matrix for n joints given by the following equation (10):

$$W_p = \begin{bmatrix} W_{p1} & 0 & \cdots & 0 \\ 0 & W_{p2} & \cdots & 0 \\ \vdots & \vdots & \ddots & \vdots \\ 0 & 0 & \cdots & W_{pn} \end{bmatrix} , (10)$$

The weight least normal solution with left hand joint velocity, $\dot{x}$ is given in equation (11):

$$V_{wm} = W_p^{-1} J^T \left[J W_p^{-1} J^+ \right]^{-1} \dot{x} , (11)$$

where J is a $6 \times n$ full rank space Jacobian for non-coordinated tasks and relative Jacobian for coordinated tasks. The performance factor $L(\theta)$ for avoiding the joint limits for angle θ_i with maximum and minimum joint limits θ_{max} and θ_{min} is given in the following equation (12):

$$L(\theta) = \sum_{i=1}^{n} \frac{1}{4} \frac{(\theta_{max} - \theta_{min})^2}{(\theta_{max} - \theta_i)(\theta_i - \theta_{min})} , (12)$$

where the value of $L(\theta)$ was higher when located closer to the joint limits, becomes the infinity at the joint limits and one at a middle range from the joint limits. The elements of W_p are given in the following equation (13):

$$W_{pi} = 1 + \left| \frac{\partial L(\theta)}{\partial \theta} \right| , (13)$$

where $\frac{\partial L(\theta)}{\partial \theta}$ is the joint limit gradient potential function given in the equation (14):

$$\frac{\partial L(\theta)}{\partial \theta} = \frac{(\theta_{\max} - \theta_{\min})^2 (2\theta - \theta_{\max} - \theta_{\min})}{4(\theta_{\max} - \theta_j)^2 (\theta_j - \theta_{\min})^2} , (14)$$

The gradient function became zero when joint, i was at the middle range of the joint limits and infinity at both extreme joint limits (and hence the joint velocity reduced). The joint limit penalty function by considering all the joints of the redundant arms with scaling coefficient, k is given in the following equation (15):

$$W_p = 1 - \exp(-k \prod_{i=1}^{n} \frac{(\theta_{\max} - \theta_j)(\theta_j - \theta_{\min})}{(\theta_{\max} - \theta_{\min})^2} , (15)$$

The performance penalty function ranged from zero to one. The value of penalty function decreased to zero at the joint limits and became one at the mid-range. The penalty terms for joint limits based on the range of joints are summarized in the following equation (16):

$$W_{pi} = \begin{cases} W_{pi}^- = \begin{cases} 1, \left| (\theta_i - \theta_{\min}) \right| > \left| \theta_{\max} - \theta_i \right| \\ 1 + \left| \frac{\partial L(\theta)}{\partial \theta} \right|, otherwise \end{cases} \\ W_{pi}^+ = \begin{cases} 1 + \left| \frac{\partial L(\theta)}{\partial \theta} \right|, \left| (\theta_i - \theta_{\min}) \right| > \left| \theta_{\max} - \theta_i \right| \\ 1, otherwise \end{cases} \end{cases} , (16)$$

The penalty terms W_{pi}^- and W_{pi}^+ represent the joint limit penalty function applied during negative and positive directions (clockwise and anti-clockwise directions) respectively. The penalty function value compensating joint angle ranges became one when the current joint angle was in the upper half of the joint angle range. Hence, the penalty function was multiplied along with the Jacobian only when the joint angle range was above the upper half of the angle range.

4.2 Obstacle penalty function

The presence of obstacles in a robot's workspace limits the robot manipulability. Let d_m be a minimum distance between two points p'_m and p'_o on outermost surfaces of the end-effector and an obstacle respectively. The distance d between the manipulator and the obstacles is given in equation (17):

$$p_o^{'} - p_m^{'} = d , (17)$$

Distance d should be greater than d_m to avoid collisions. Consider a collision function $f(\theta, d)$, which becomes zero at a maximum distance and attains a maximum value at $d < d_m$. Then the collision function gradient ∇f is given in equation (18):

$$\nabla f = \frac{\partial f}{\partial \theta} = \frac{\partial f}{\partial d} \times \frac{\partial d}{\partial \theta} , (18)$$

Function $f(\theta, d)$ [26] given in equation (19) was selected in such a way that the function gradient ∇f becomes zero when distance, d becomes larger and becomes infinity when d approaches zero:

$$f(\theta, d) = \rho e^{-\alpha d} d^{-\beta} , (19)$$

where α and β are the parameters controlling rate of decay; the values of α and β are computed based on an obstacle and an assigned task [26]. The decay amplitude is determined by parameter ρ that is given in the following equation (20):

$$\frac{\partial f(\theta)}{\partial d} = -\rho e^{-\alpha d} d^{-\beta} (\beta d^{-1} + \alpha) , (20)$$

The change in d with respect to changes in joint angles is given in the following equation (21):

$$\frac{\partial d}{\partial \theta} = \frac{1}{d} [J_a^T (p_{va} - p_{vb}) + J_b^T (p_{vb} - p_{va})]^T , (21)$$

where p_{va} and p_{vb} represent position vectors corresponding to two collision points and associated Jacobians, J_a and J_b. The collision penalty function can be summarized in positive and negative directions in the following equation (22):

$$O_{pi} = \begin{array}{l} O_{pi}^{-} = \left\{ \begin{array}{l} 1, \Delta|\forall f_i| \geq 0 \\ 1 + \Delta|\forall f_i|, otherwise \end{array} \right\} \\ O_{pi}^{+} = \left\{ \begin{array}{l} 1 + \Delta|\forall f_i|, \Delta|\forall f_i| \geq 0 \\ 1, otherwise \end{array} \right\} \end{array}, (22)$$

The change of magnitude of the collision gradient function is given by $\Delta|\nabla f_j|$. A positive value indicated joints' motion towards a collision, while a negative value indicated a motion away from the collision. The weight factor value became very large and turned into the infinity when distance between the manipulator and obstacles decreased below d_m. An increase of the weight factor value reduced the joint velocity and prevented the motion of arm towards that particular direction. The collision penalty function for the upper body humanoid robot is given in the following equation (23):

$$O_p = \frac{1}{n} \sum_{i=1}^{n} O_{pi}, (23)$$

4.3 Determining Augmented relative Jacobian matrix

The Augmented Jacobians for non-coordinated and coordinated tasks are given in equations (24) and (25) respectively:

$$J_{aug} = W_p O_p J_f, (24)$$

$$\text{where, } J_f = \left\{ \begin{array}{l} J_m, non-coordinated \\ J_R, coordinated \end{array} \right\}, (25)$$

The workspace was divided into hyperoctants of 2^6 divisions. Each hyperoctant ranges from (-1 to +1). Equations (24) and (25) are decomposed using the Singular value decomposition (SVD) method to compute singular values. These singular values were the corresponding eigenvalues of each hyperoctant. There existed two orthogonal matrices related to the Augmented Jacobian matrix, $J_{aug}{}^{mxn}$ as given in the following equation (26):

$$J_{aug} = UA'B^T, (26)$$

where U and B^T are orthogonal matrices with order m×r and r×n respectively, and A' is given in the following equation (27):

$$A' = \begin{bmatrix} \delta & 0 \\ 0 & 0 \end{bmatrix}, (27)$$

with $\delta = diag(\lambda_1, \lambda_2, ... \lambda_r)$, which represents the singular values of J_{aug} or the orthonormal eigenvectors of $J_{aug}{}^T J_{aug}$. The Jacobian matrix in terms of Eigen values is given in the following equation (28):

$$J_{aug} = \lambda_1 \times \lambda_2 \times .... \lambda_r, (28)$$

The extended inverted condition number, C_{ext} by considering the Augmented Jacobian is calculated using the following equation (29):

$$C_{ext} = \frac{\min(S_\Gamma)}{\max(S_\Gamma)}, (29)$$

where S_Γ represents a new set of eigenvalues corresponding to each hyperoctant. C_{ext} considered redundancy conditions of manipulators, since redundant joints penalized joint limit values occurring in motion with the help of its kinematic model. These eigen values and corresponding eigen vectors were used for computing the manipulability measurements and analyzing the corresponding manipulability and the force ellipsoids to study the range of motions.

5. Results and discussion

This paper presented the manipulability analysis of an upper-body humanoid robot with a wheeled base. Manipulability measurements of various configurations of dual arms doing cooperative and non-cooperative tasks were determined. Space Jacobian and relative Jacobian of the upper body section formulated based on the screw theory formulation were used for determining manipulability measurements of non-cooperative and cooperative tasks respectively. These manipulability measurements incorporating effects of obstacles and joint limits were used for optimising the joint configurations of upper body of humanoid robot avoiding joint limits and obstacle collisions. The flowchart of methodology adopted in this work to determine the joint solutions of redundant arms for carrying out cooperative and non-cooperative task are shown in figure 4.

Cubic spline trajectory for carrying out the prescribed task were optimised based on energy consumed and time duration of completion of task. Joint solutions for traversing the finalised trajectory were determined and manipulability ellipsoids were plotted for each configuration of redundant arms using Augmented Jacobian. The direction of major axis of obtained manipulability ellipsoid for each configuration was compared with the direction of major axis of desired manipulability ellipsoid. A similarity index, S_{index} is derived as given in equation (30).

$$S_{index} = \frac{\theta_{des} - \theta_{obt}}{\left\| \theta_{des} \right\| \left\| \theta_{obt} \right\|} , (30)$$

where, θ_{des} and θ_{obt} represent direction vectors of major axis of desired manipulability ellipsoid and obtained manipulability ellipsoid respectively. S_{index} values close to 1 were chosen for finalising various configurations for traversing the determined trajectory. Manipulability measurements obtained using equation (4) for non-cooperative tasks and equation (8) for cooperative tasks are used for determining the volume of manipulability ellipsoid. The joint configurations were updated until the obtained manipulability ellipsoids matched with desired manipulability ellipsoids. The proposed methodology ensured that the resulting joint solutions were not at the extreme limits, avoids collision with obstacles and reduced self-collision chances.

5.1 Manipulability and force ellipsoid for non-coordinated tasks using Augmented Jacobian
Simulations were carried out for evaluating the performance of coordinated and non-coordinated tasks using the proposed approach. Left hand was assumed to be moving through a cubic spline trajectory (blue colour) inside the workspace consisted of obstacle as shown in figure 5. The trajectory was updated (red colour) using the collision avoidance technique proposed in [34].

After optimising the trajectory, desired manipulability and force ellipsoids are constructed through the trajectory coordinates as shown in figure 6. Joint configurations of left arm for traversing the given trajectory were obtained as shown in figure 7 using an improvised Levenberg-Marquardt method [38]. Joint configurations were updated until the direction of major axes of obtained and desired manipulability ellipsoids were similar. When calculating joint configurations to traverse given trajectory by satisfying above mentioned criterion, extreme joint values were avoided from the joint sets using joint limit penalty function. Additionally, coordinates of obstacle regions were omitted from the trajectory coordinates by using obstacle avoidance penalty function. Force ellipsoids were generated perpendicular to manipulability ellipsoids, hence force ellipsoids also get aligned with updated manipulability ellipsoids. Similarity index of ellipsoids was obtained in the range of 0.93 - 0.97.

Joint solutions of left arm during the motion depicted in figure 7 is shown in figure 8. Comparison of volume of manipulability ellipsoids for the particular task determined using conventional (without including penalty function) and proposed approaches is obtained as shown in figure 9. Manipulability measurement using proposed approach was obtained less as compared to conventional approach due to the presence of obstacle and joint limits. Conventional approach calculated manipulability measurement without considering obstacle regions and extreme joint values. Hence, manipulability measurements were higher using conventional approach compared to proposed approach. The redundant arm reached the middle of the workspace in 5 seconds from the beginning of the motion and hence showcased maximum manipulability measurement due to the maximum range of motion possible for the arm.

5.2 Manipulability analysis of redundant arms for non-coordinated and coordinated tasks
The humanoid upper body with mobile platform was simulated for evaluating the coordinated motion capabilities of the combined mechanism. The assigned task consisted of both non-coordinated and coordinated tasks. Non-coordinated tasks were evaluated using Augmented Jacobian derived in equation (24) and coordinated task using equation (25). The task was assigned in such a way that the wheeled humanoid was placed initially at a location away from the table and it moved to the table location to grasp a cup placed on a table. The mobile platform stopped in front of the table by keeping a safe distance with the cup. Screenshots of different poses of hand end effectors for picking the cup are shown in figure 10. The table was considered as an obstacle during the motion and joint limits and self-collision chances were considered while performing the task. The motion of the arms and desired manipulability ellipsoids for picking up the cup and corresponding ellipsoids are shown in figure 9. Screenshots 1 and 2 show the non-coordinated motions of redundant arms and after reaching the cup the redundant arm traverses the trajectory with coordinated motions to raise the cup as shown in screenshot 3.

The trajectory of left arm for picking up the cup and ellipsoids are shown in figure 11. Various joint configurations determined for the desired manipulability ellipsoids are shown in figure 12. Joint angles of left arm for traversing the trajectory shown in figure 12 are shown in figure 13. The joint configurations were updated until the major axes directions of the obtained and desired manipulability ellipsoids became identical. When calculating joint configurations to traverse a given trajectory, the joint limit penalty function was used to exclude extreme joint values from the joint sets. Furthermore, the implementation of obstacle avoidance penalty function removed the coordinates of obstacle areas from the trajectory coordinates. Comparison of manipulability ellipsoid measurements obtained using conventional and proposed method are shown in figure 14. At initial stage, the manipulability was less for the arms due to the pose of redundant arm near the workspace boundary. Manipulability measurements of redundant arms decreased in 5 seconds from the beginning of the motion due to the presence of obstacle (a table) inside the workspace and joint solutions near to extreme joint values. And later the manipulability increased due to the joint configurations were obtained at mid-range joint values and no presence of obstacles at the current region of workspace. Similarity index of ellipsoids was obtained in the range of 0.92-0.98. Figure 15 shows the experimental set up and motions of the humanoid robot to grasp the cup. Screen shot 1 is the starting location and screenshot 2 represents the end location. ArUCO markers [33] were used for recording the poses of the humanoid robot. The various poses of arms for grasping the cup are shown in figure 16. After reaching the given location measured using ArUCO markers, the dual arms were operated to pick up the cup placed on the table as shown in screenshots 1 - 4. The redundant arms were moved together to grasp the cup from the table. The end effector grippers were given only to the left hand and the right hand supported the cup. Screen shot 1 shows the initial pose of humanoid robot in front of the table where the cup is placed. In screen shot 2, the dual arms were moving towards the cup and screenshots 3 and 4 represent the grasping phases. The implementation of joint solutions obtained from simulations enabled the motion of the humanoid redundant arms excluding extreme joint angles and collision issues. The experimental validation of proposed approach by feeding the humanoid upper body joints with optimised joint solutions also verified the real time efficiency of the method.

6. Conclusion

Manipulability analysis of complex systems like the humanoid robot is a challenging task due to its complex nature. A better manipulability analysis method enhances a humanoid robot performance by verifying and evaluating different dexterous configurations inside a robot's workspace. This paper presented the manipulability analysis of a tree-type upper body wheeled mobile humanoid robot with dual redundant arms. A methodology for updating joint solutions avoiding joint limits and obstacle regions for completing cooperative and non-cooperative tasks was presented using the proposed manipulability approach. Manipulability analysis using a derived penalty function determined the dexterity of the redundant dual arms more effectively for various hand configurations as compared to conventional method. The penalty function derived in this work was used to manipulate the characteristics near various joint limits as well as for avoiding obstacles and self-collision chances. The computational time for determining relative Jacobian was less due to the change only in the rotational and wrench transformation matrix when changing the direction of motion of joints. The joint solutions were finalized when similarity index value was obtained over 0.9. However, when redundant arms were taking sharp turns the ellipsoids similarity index was obtained in the range of 0.8 - 0.9. Hence, future research works will be focused on reducing the above-mentioned issue to increase the performance of the proposed manipulability analysis. The manipulability capabilities of the redundant arms were tested and the proposed model was experimentally validated. The proposed manipulability measurements can be extended to analyse the dynamics of humanoid robot. The fabricated humanoid robot could be further improved by designing a stable intelligent controller that incorporates a speech recognition, an image processing, an artificial intelligence and other techniques.

Author contributions

Shifa Sulaiman conceived the presented idea, developed the theory and performed computations. She also performed experimental validations and wrote the manuscript. Sudheer A P verified analytical and experimental results of the work. He also supervised the findings of the work and supported manuscript corrections. Santhakumar Mohan assisted in drafting the manuscript. Evgeni Magid provided critical feedback and assisted in manuscript corrections.

Funding source

References

[1] Shah, J., Wiken, J., Williams, B., et al. "Improved human-robot team performance using chaski, a human-inspired plan execution system", In *Proceedings of the 6th international conference on Human-robot interaction,* pp. 29-36 (2011).

[2] Díaz-Boladeras, M., Paillacho, D., Angulo, C., et al. "Evaluating group-robot interaction in crowded public spaces: A week-long exploratory study in the wild with a humanoid robot guiding visitors through a science museum", *International Journal of Humanoid Robotics*, 12(04), (2015).

[3] Karar, A. S., Said, S., and Beyrouth, T. "Pepper humanoid robot as a service robot: A customer approach." In *2019 3rd International Conference on Bio-engineering for Smart Technologies (BioSMART)*, pp. 1-4 (2019).

[4] Lee, M. K., Forlizzi, J., Rybski, P. E., et al. "The snackbot: documenting the design of a robot for long-term human-robot interaction." In *Proceedings of the 4th ACM/IEEE international conference on Human robot interaction*, pp. 7-14 (2009).

[5] Mišeikis, J., Caroni, P., Duchamp, P., et al. "Lio-a personal robot assistant for human-robot interaction and care applications." *IEEE Robotics and Automation Letters* 5, pp. 4 (2020).

[6] Graf, B., and Eckstein, J. "Service Robots and Automation for the Disabled and Nursing Home Care." In *Springer Handbook of Automation*, Cham: Springer International Publishing, pp. 1331-1347 (2023).

[7] Morris, K.J., Samonin, V., Baltes, J., et al. "A robust interactive entertainment robot for robot magic performances." *Applied Intelligence* 49, pp. 3834-3844 (2019):.

[8] Retto, J. "Sophia, First Citizen Robot of the World," *Univ. Nac. Mayor San Marcos*, (2017).

[9] Ambrose, R. O. "Development and deployment of robonaut 2 to the international space station." In *ICRA 2011 (International Conference on Robotics and Automation*, (2011).

[10] Dwarakanath, N. "Gaganyaan mission: meet Vyommitra, the talking human robot that ISRO will send to space." *India Today* 22 (2020).

[11] Rastegarpanah, A., Aflakian, A., and Stolkin, R. "Improving the manipulability of a redundant arm using decoupled hybrid visual servoing." *Applied Sciences* 11, 23 (2021).

[12] Neha, E., and Shrivastava, Y. "Analysis of manipulability for a robotic hand using statistical approach." *Materials Today: Proceedings* 43, pp. 164-168 (2021).

[13] Patel, S., and Sobh, T. "Task based synthesis of serial manipulators.," *Journal of advanced research* 6(3), pp. 479-492 (2015) .

[14] Freddi, A., Longhi, S., Monteriù, A., et al. "Redundancy analysis of cooperative dual-arm manipulators," *Int. J. Adv. Robot. Syst.*,13(5), pp. 1–14 (2016).

[15] Chan, T.F., and Dubey, R.V. "A weighted least-norm solu-tion based scheme for avoiding joint limits for redundant joint manipulators", IEEE Transactions on Robotics and Automation. 11(2), pp. 286-92 (1995).

[16] Ferreira, N.F. and Machado, J.T. "Manipulability analysis of two-arm robotic systems," *4th IEEE Int. Conf. Intell. Eng. Syst.*, pp. 101–109 (2000).

[17] Zhang, S., Ouyang, B., He, X., et al. "Face Tracking Strategy Based on Manipulability of a 7-DOF Robot Arm and Head Motion Intention Ellipsoids," *IEEE Int. Conf. Real-Time Comput. Robot,* pp. 290–295 (2022).

[18] Chiriatti, G., Bottiglione, A. and Palmieri, G. "Manipulability Optimization of a Rehabilitative Collaborative Robotic System," *Machines*, vol. 10(6), pp. 1–11 (2022).

[19] Choi, Y.S., Rhee, I., Hoang, P.T. and Choi, H.R. "Simple desired manipulability ellipsoid with velocity and force for control of redundant manipulator," *J. Mech. Sci. Technol.*, 37(4), pp. 2033–2041 (2023).

[20] Torabi, A., Khadem, M., Zareinia, K., et al. "Manipulability of teleoperated surgical robots with application in design of master/slave manipulators," *Int. Symp. Med. Robot. ISMR,* , pp. 1–6 (2018).

[21] Lachner, J., Schettino, V., Allmendinger, F., et al. "The influence of coordinates in robotic manipulability analysis", Mechanism and machine theory, 146, (2020).

[22] Chen, C., Wang, X., Chen, H., et al. "Analysis of singular configuration of robotic manipulators", Electronics, 10(18), (2021).

[23] Zhu, Q., Tian, M., Liu, Q., et al. "Design, kinematics and manipulability analyses of a serial-link robot for minimally invasive treatment in femoral shaft fractures"., Journal of Mechanics in Medicine and Biology, 22(09) (2022).

[24] Akli, I. "Trajectory planning for mobile manipulators including manipulability percentage index", *International Journal of Intelligent Robotics and Applications,* 5(4), 543-557 (2021).

[25] Dufour, K. and Suleiman, W. "On maximizing manipulability index while solving a kinematics task.", *Journal of Intelligent & Robotic Systems* 100 pp. (3-13) (2020).

[26] Vahrenkamp, N., Asfour, T., Metta, G., et al. "Manipulability analysis", In *12th ieee-ras international conference on humanoid robots,* pp. 568-573 (2012).

[27] Bicchi A, Melchiorri C. and Balluchi D. "On the mobility and manipulability of general multiple limb robots", IEEE Transactions on Robotics and Automation, 11(2), pp. 215-28 (1995).

[28] Shen, Y., Hsiao, B.P.Y., Ma, J., et al. "Upper limb redundancy resolution under gravitational loading conditions: Arm postural stability index based on dynamic manipulability analysis," In *IEEE-RAS Int. Conf. Humanoid Robot.*, pp. 332–338 (2017)

[29] Kumar, R. and Mukherjee, S. "Algorithmic Selection of Preferred Grasp Poses Using Manipulability Ellipsoid Forms," *J. Mech. Robot.*,14(5), pp. 1–24 (2022).

[30] Rozo, L., Jaquier, N., Calinon, S., et al. "Learning manipulability ellipsoids for task compatibility in robot manipulation," *IEEE Int. Conf. Intell. Robot. Syst.*, pp. 3183–3189 (2017).

[31] Vahrenkamp, N. and Asfour, T. "Representing the robot's workspace through constrained manipulability analysis". Autonomous Robots, 38(1), pp.17-30 (2015).

[32] Albers, A., Brudniok, S., Ottnad, J., et al. "Upper body of a new humanoid robot-the design of ARMAR III", In 6th IEEE-RAS International Conference on Humanoid Robots, pp. 308-313 (2006).

[33] Sulaiman, S. and Sudheer, A.P. "Dexterity analysis and intelligent trajectory planning of redundant dual arms for an upper body humanoid robot". Industrial Robot: the international journal of robotics research and application, 48(6), pp.915-928 (2021).

[34] Sulaiman, S., and Sudheer, A. P. "Modeling of a wheeled humanoid robot and hybrid algorithm-based path planning of wheel base for the dynamic obstacles avoidance", Industrial Robot: the international journal of robotics research and application, 49(6), (2022).

[35] Winter DA. "Biomechanics and motor control of human movement", John Wiley & Sons, (2009).

[36] Lynch K.M., and Park F. "*Modern Robotics -Mechanics, Planning, and Control*", (2017).

[37] Jamisola Jr R.S., Mastalli C and Ibikunle F. "Modular relative jacobian for combined 3-arm parallel manipulators", International Journal of Mechanical Engineering and Robotics Research, 5(2) pp. 90-5 (2016).

[38] Fu, Z., Han, B., and Chen, Y. "Levenberg–Marquardt method with general convex penalty for nonlinear inverse problems", Journal of Computational and Applied Mathematics, 404, (2022).

Author Biographies

Shifa Sulaiman: Dr. Shifa received her Master's degree in Machine Design from the Mahatma Gandhi (MG) University, India in 2013. From 2013-2017, Shifa worked as an Assistant Professor in various Indian Engineering Institutes. Shifa earned her PhD from the National Institute of Technology, Calicut, India in 2023. She is currently working as a Research Associate at the Laboratory of Intelligent Robotic Systems (LIRS) at Kazan Federal University, Russia. Her research interests include design, modelling, path planning and trajectory planning of mobile robots.

Sudheer A P: Dr. Sudheer. A. P is currently working as Associate Professor, in the Mechanical Engineering department, National Institute of Technology Calicut (NITC). He earned his PhD from the NITC and he is a member of "Robotics Society India"(TRS-India) and ISTE. Presently he is the editor of TRS India. He has published peer reviewed journals, conferences and patents. His research interests include modelling, analysis, path planning, trajectory planning and control of robots.

Santhakumar Mohan: Prof. Santhakumar Mohan earned his Ph.D. (Robotics and Control) from the Indian Institute of Technology Madras, Chennai (India) in 2010. He is serving as Technical Editor, of IEEE/ASME Transactions on Mechatronics, Associate Editor, of IEEE Robotics and Automation Letters, ASME Letters in Dynamic Systems and Control, and Robotica. He is also an adjunct professor at the Department of Engineering Design, at IIT Madras and a Faculty Fellow at the IIT Palakkad Technology IHub Foundation (IPTIF). His research interests include modelling and control of robots.

Evgeni Magid: Prof. Evgeni Magid is the head of Intelligent Robotics Department and Laboratory of Intelligent Robotic Systems (LIRS) at Kazan Federal University, Russia. He is also working as a Professor at HSE University, Russia and a Senior IEEE member. Previously he worked at University of Bristol, UK; Carnegie Mellon University, USA; University of Tsukuba, Japan; National Institute of Advanced Industrial Science and Technology, Japan. He earned his Ph.D. degree from the University of Tsukuba, Japan. His research interests include human-robot interaction, modelling and path planning algorithms of mobile robots

List of Tables

List of Figures

Table

Table 1. Length of various links

Dimensions	Length(m)
L1	0.438
LH	0.276
L3 & L3'	0.196
L4 & L4'	0.282
L5 & L5'	0.152
LE & LE'	0.260

Figures
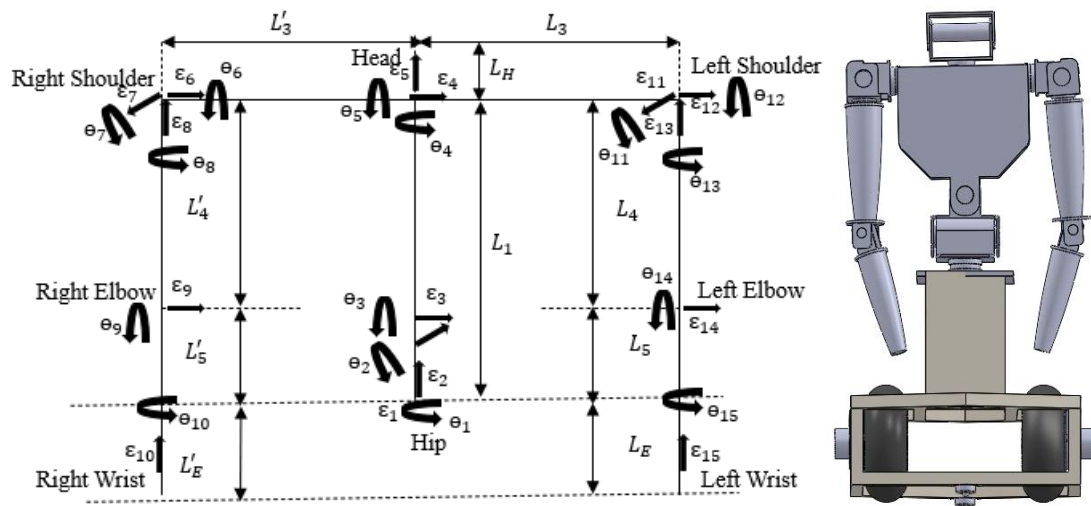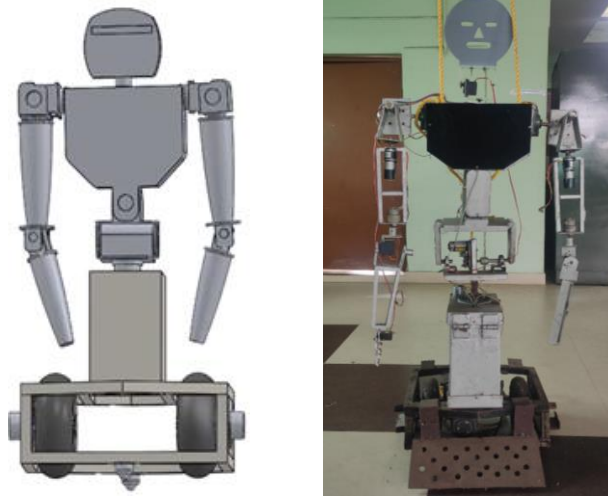
(a)   (b)
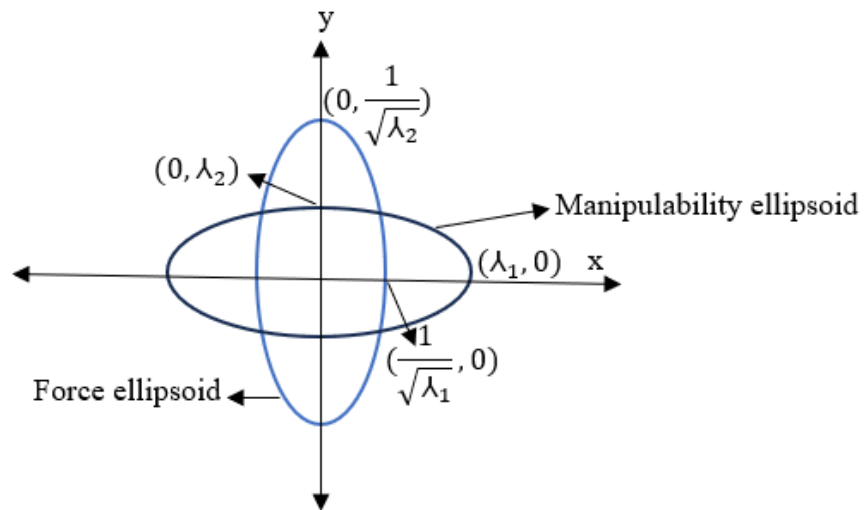Figure 2. Wheeled humanoid robot with a wheeled base: (a) conceptual model (b) fabricated model

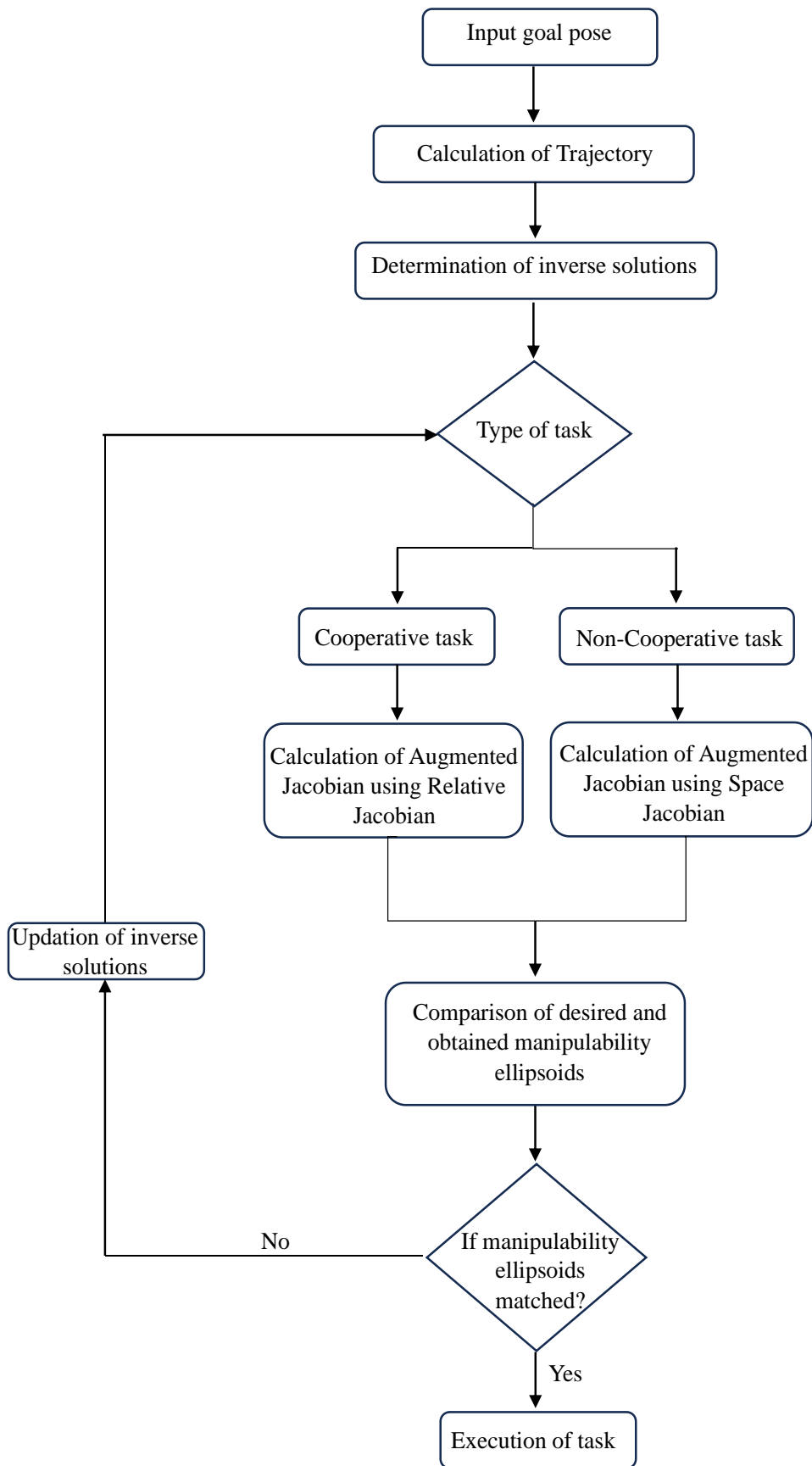Figure 3. Representation of the force ellipsoid and the manipulability ellipsoid
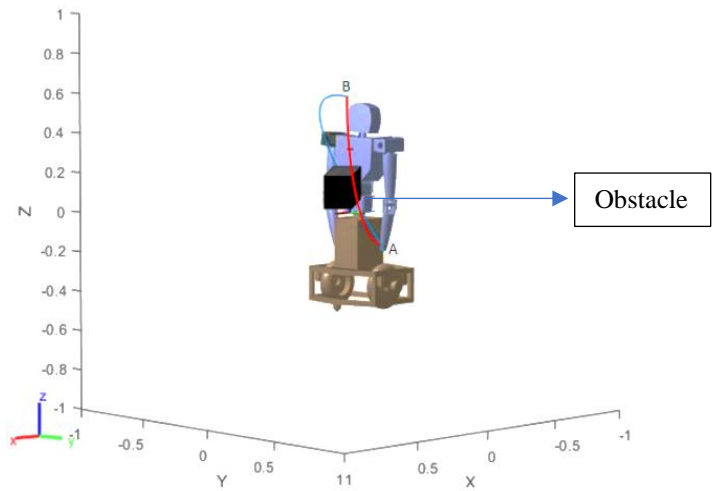
Figure 4. Flowchart of proposed manipulability analysis methodology

Figure 5. Comparison of trajectories
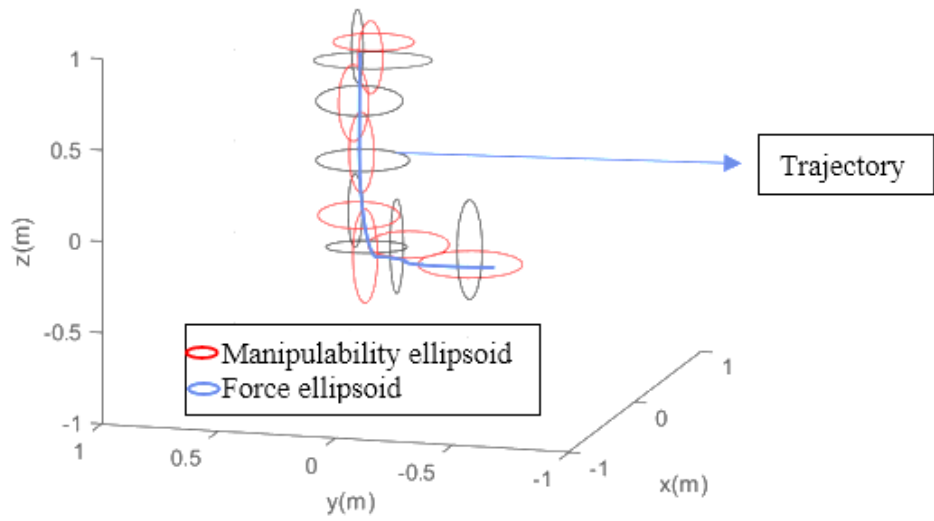
Figure 6. Desired manipulability and force ellipsoids constructed through trajectory
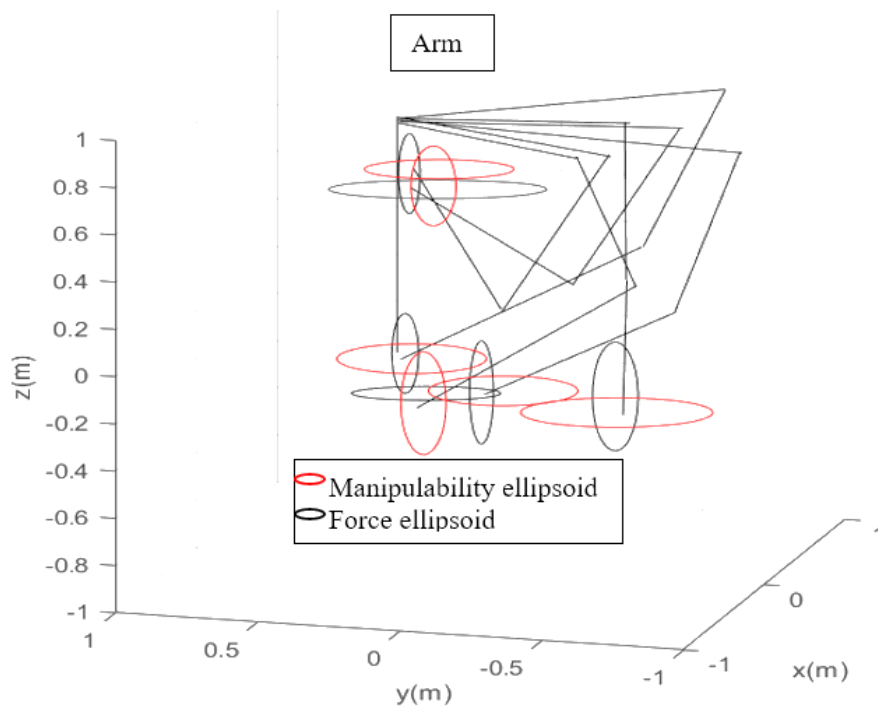
Figure 7. Joint configurations of left arm
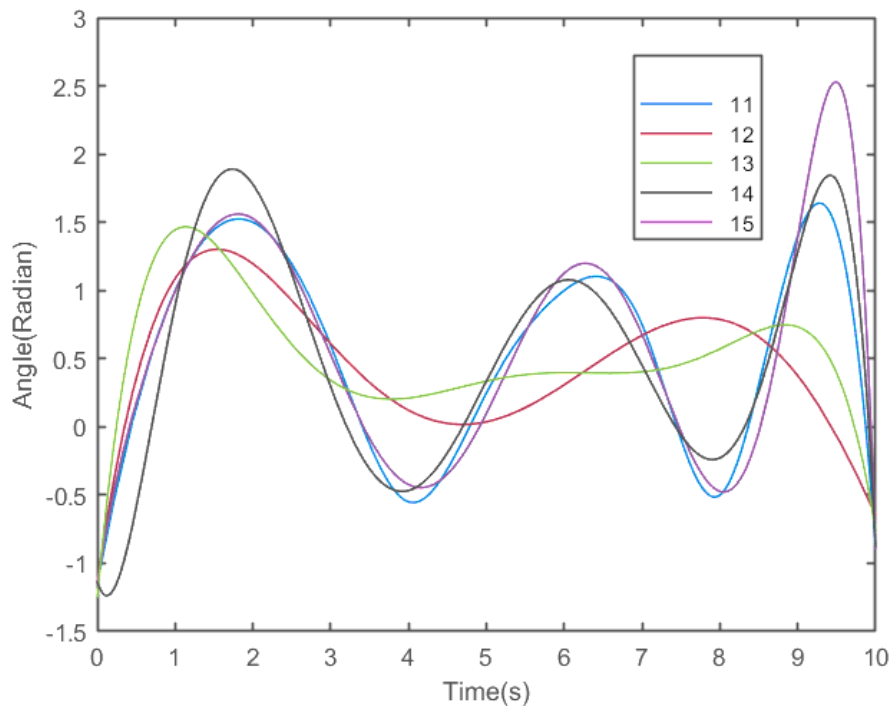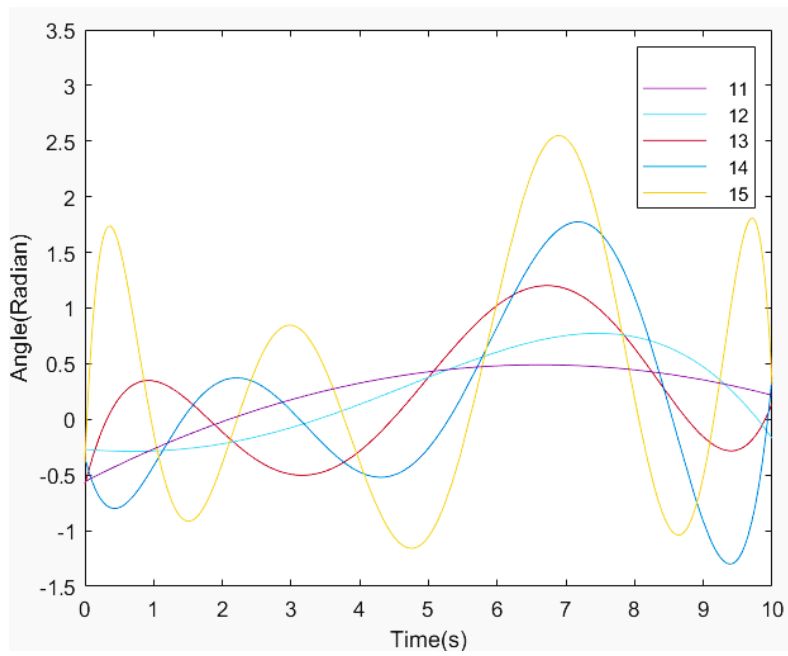

Figure 8. Joint angles of left arm
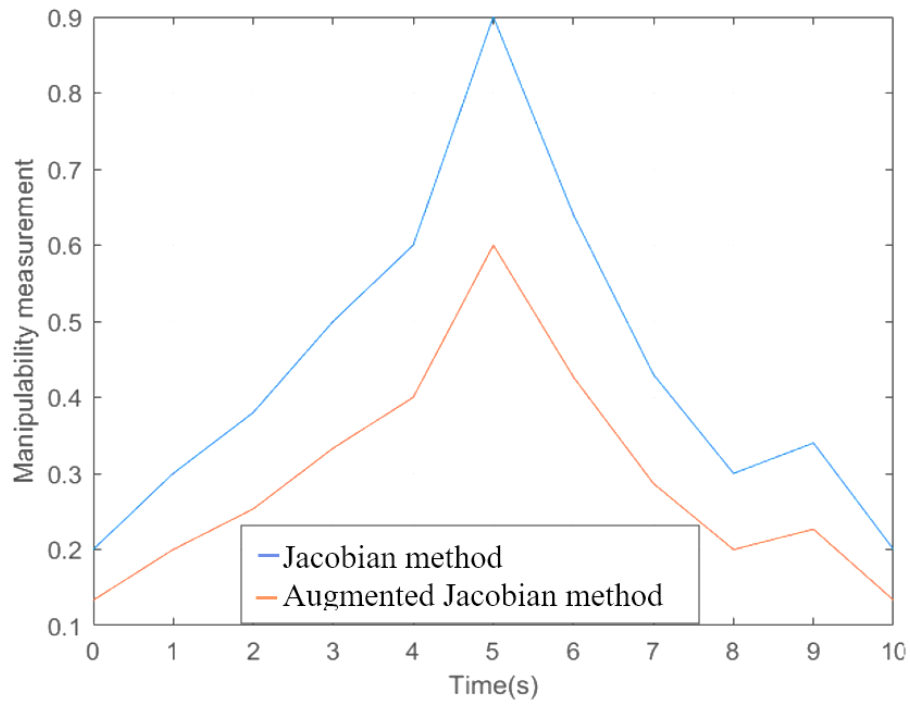
Figure 9. Comparison of manipulability measurement obtained from Jacobian and proposed Augmented Jacobian methods for non-coordinated task
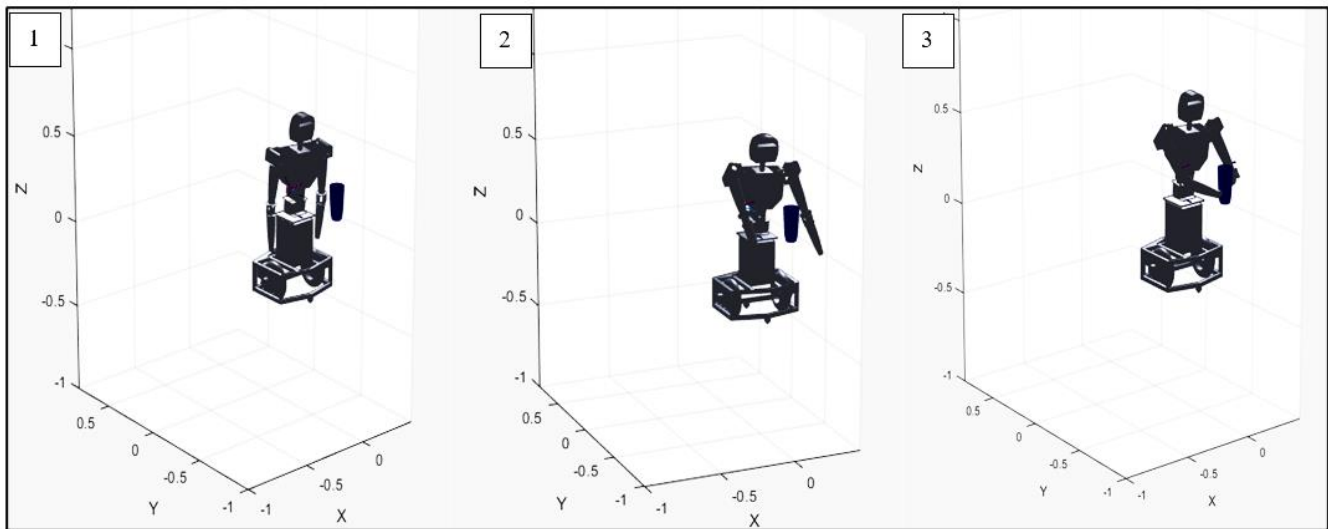
Figure 10. Different poses of hand end effector for picking a cup
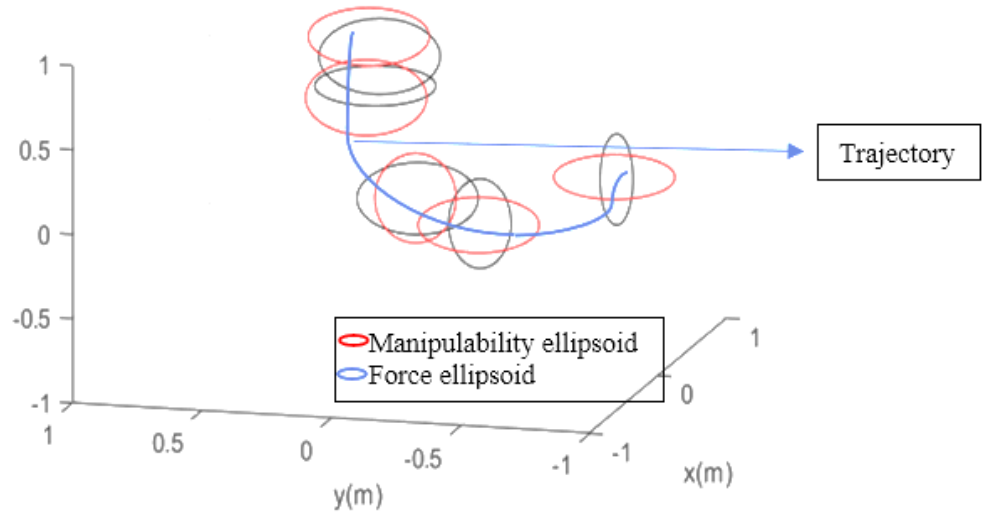
Figure 11. Desired manipulability and force ellipsoids for redundant arms
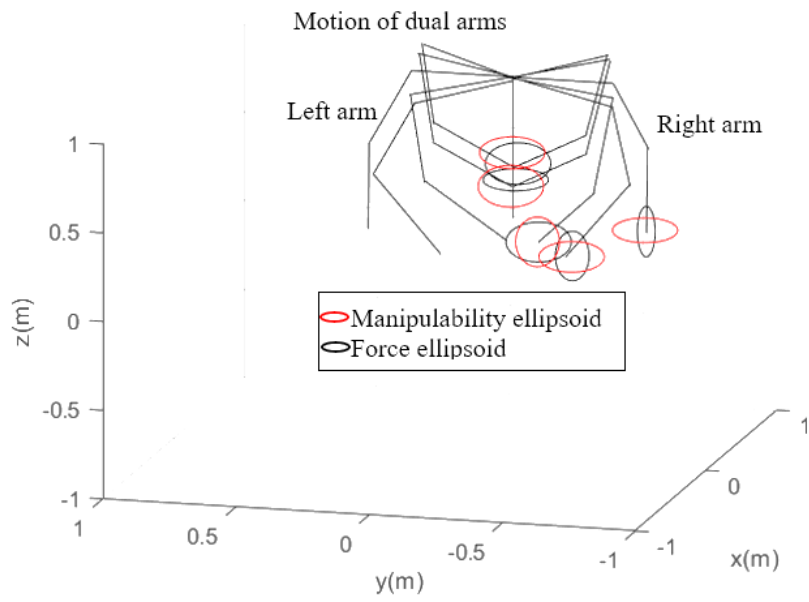
Figure 12. Manipulability and force ellipsoids corresponding to each configuration of arm to picking up the cup

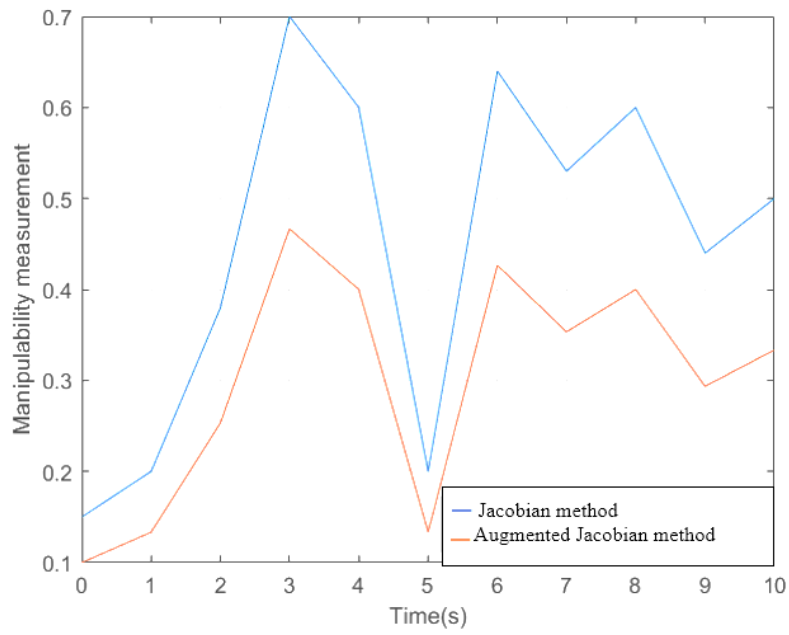Figure 13. Joint angles of left arm during coordinated motion

Figure 14. Comparison of manipulability measurement obtained from Jacobian and proposed Augmented Jacobian methods for redundant arms
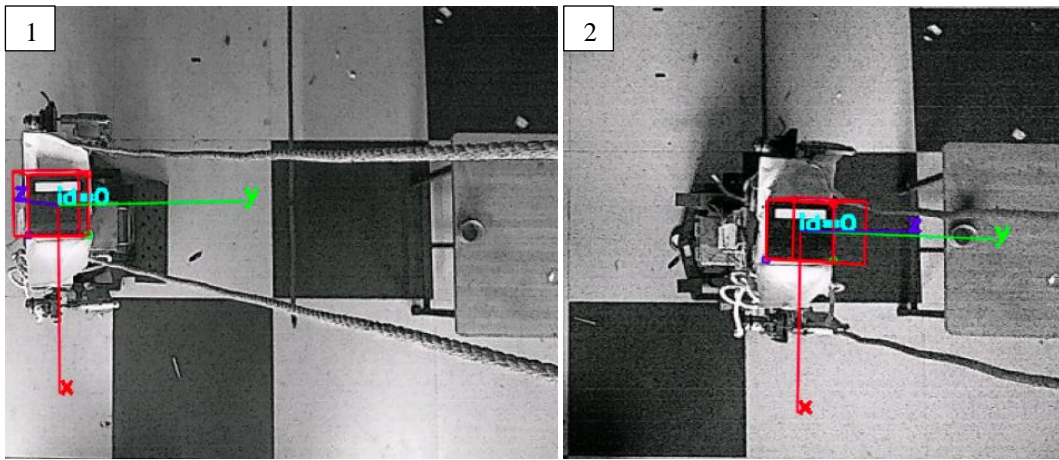
Figure 15. Motion of humanoid robot to reach the location
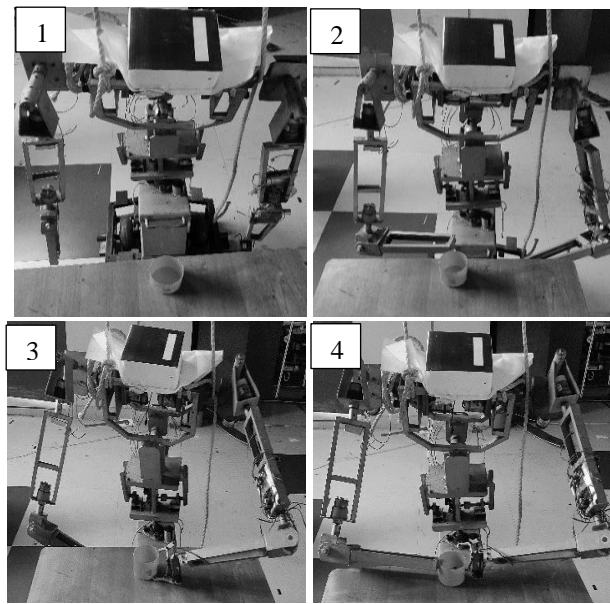

Figure 16. Various poses of hand effectors for picking up the cup from the table